

Neutron star properties: Constraining the nuclear matter EoS

Constança Providência^{1,a)}

^{a)}Corresponding author and speaker: cp@uc.pt

¹*CFisUC, Department of Physics, University of Coimbra, 3004-516 Coimbra, Portugal*

Resumo. We examine the influence of the density dependence of the symmetry energy on several properties of neutron stars. In particular, we study the constraints set on the nuclear matter equation of state by the values of the tidal deformability and neutron star radius, using a diverse set of relativistic and non-relativistic mean field models consistent with bulk properties of finite nuclei and the observed lower bound on the maximum mass of neutron star. The tidal deformability and radius show a strong correlation with specific linear combinations of the isoscalar and isovector nuclear matter parameters associated with the EoS. Such correlations suggest that a precise value of the radius or the tidal deformability can put tight bounds on several EoS parameters, in particular, on the slope of the incompressibility and the curvature of the symmetry energy. We show that the density dependence of the symmetry energy has a direct influence on the amount of strangeness inside cold dense matter and, consequently, on the direct Urca process and cooling of neutron stars. We explain the low luminosity of SAX 1808.4-3658 as a result of hyperonic direct Urca processes. Finally, we discuss the strong influence of the density dependence of the symmetry energy on the extension of the crust-core transition region of a magnetized neutron star. The increase of the crust and its of complexity, due to the magnetic field effect, may have a role on the glitch mechanism or on the magnetic field decay.

Symmetry energy and neutron star properties

The density dependence of the symmetry is affecting strongly the properties of asymmetric nuclear matter, including nuclear properties and neutron star properties as the neutron skin thickness of the nucleus, the neutron star radius or the onset of the Urca process inside neutron stars, see [1] for a review. In the following, we will discuss how the symmetry energy dependence on the density determines neutron star properties as its radius or tidal deformability, or affects properties of hyperonic stellar matter [2, 3, 4] and of magnetized nuclear matter [5, 6] .

The symmetry energy is reasonably well constrained at saturation or sub-saturation densities, see [7, 8, 9], but little is known about its behavior at high densities. The existence of correlations between the EoS properties and NS properties dependent on the behavior of the EoS at large densities may help constraining the high density EoS. As an example, the measurement of the radius of a $1.4M_{\odot}$ NS star or its tidal deformability with a small uncertainty would certainly impose strict constraints on the high density EoS of asymmetric nuclear matter. In particular, the recent detection of gravitational waves from a binary neutron star merger, the GW170817 event [10, 11], has boosted a large discussion on this topic, see for instance [12, 13, 14, 15, 16, 17, 18, 19].

To describe neutron stars, the EoS state of stellar matter must be known in the whole range of densities of relevance. Hyperons may occur in the NS because its appearance will lower the energy of the system. Since some of the hyperonic species have a non-zero isospin, the symmetry energy will also affect the onset and abundance of these hyperons [3], and as a consequence, other properties as the onset of the direct Urca process. A second problem we will discuss in the following is the interplay between the symmetry energy properties and the hyperon content of the star.

Since the measurement of two solar mass NS, PSR J1614 – 2230 [20, 21] and PSR J0348 + 0432 [22], it has been argued that this large mass would exclude hyperons from the interior of NS because the EoS would become too soft, the “hyperon puzzle”, [23, 20, 24]. However, it has been shown that it is possible that if a hard enough EoS or an adequate choice of the hyperon-meson couplings is considered, the two solar mass constraint does not exclude hyperon inside neutron stars [25, 26, 27].

A third problem we will also discuss is how the symmetry energy defines the crust-core transition region of a magnetized neutron star. To understand the core properties of a NS it is essential to know quite well the behavior of its crust and this justifies this study. It was shown in [5, 6, 28] that a strongly magnetized star might have a complex region at the crust-core transition, which would extend the non-homogeneous range of the star to larger densities and, therefore, to deeper radii inside the star. This may have direct implications on the fractional moment of inertia of the crust and the impurity parameter of the crust [29, 30], quantities that determine the behavior of the glitch mechanism or the decay of the magnetic field [31].

Most of the study will be carried out in the framework of relativistic mean-field models (RMF) calibrated to well accepted nuclear properties resulting from neutron observations, theoretical calculations or laboratory experiments. Whenever necessary, the NS properties will be calculated from unified inner crust - core EoS since it has been shown that non-unified EoS may give rise to large uncertainties on the radius of low mass neutron stars, although essentially not affecting the mass [32]. The hyperon-meson couplings will be constrained by hypernuclei properties [33].

Brief review of the formalism

In the next section we will work with both Skyrme forces and RMF models. In the other two sections, the whole discussion will be carried out in the framework of RMF models. Within the RMF models, we consider two different sets, one including non-linear mesonic terms in the Lagrangian density, the NL set, and a second one, without these terms but introducing density dependent coupling constants, the DD set. We start from the following Lagrangian density $\mathcal{L} = \mathcal{L}_b + \mathcal{L}_m + \mathcal{L}_{m-nl}$, where the terms \mathcal{L}_b , \mathcal{L}_m , \mathcal{L}_{m-nl} describe, respectively, the baryons interacting with the mesons, the free mesons, and self-interaction and non-linear mixing terms involving mesons, these last terms only present in the NL class of models. The different terms are given by [4]

$$\mathcal{L}_b = \sum_{j=1}^8 \bar{\psi}_j \left(i\gamma_\mu \partial^\mu - m_j + g_{\sigma j} \sigma + g_{\sigma^* j} \sigma^* - g_{\omega j} \gamma_\mu \omega^\mu - g_{\phi j} \gamma_\mu \phi^\mu - g_{\rho j} \gamma_\mu \vec{\rho}^\mu \cdot \vec{I}_j \right) \psi_j, \quad (1)$$

$$\begin{aligned} \mathcal{L}_m = & + \frac{1}{2} (\partial_\mu \sigma \partial^\mu \sigma - m_\sigma^2 \sigma^2) + \frac{1}{2} (\partial_\mu \sigma^* \partial^\mu \sigma^* - m_{\sigma^*}^2 \sigma^{*2}) - \frac{1}{4} W_{\mu\nu} W^{\mu\nu} - \frac{1}{4} P_{\mu\nu} P^{\mu\nu} - \frac{1}{4} \vec{R}_{\mu\nu} \vec{R}^{\mu\nu} \\ & + \frac{1}{2} m_\omega^2 \omega_\mu \omega^\mu + \frac{1}{2} m_\phi^2 \phi_\mu \phi^\mu + \frac{1}{2} m_\rho^2 \vec{\rho}_\mu \cdot \vec{\rho}^\mu, \end{aligned} \quad (2)$$

$$\mathcal{L}_{m-nl}(\sigma, \omega_\mu \omega^\mu) = -\frac{1}{3} g_2 \sigma^3 - \frac{1}{4} g_3 \sigma^4 + \frac{1}{4} c_3 (\omega_\mu \omega^\mu)^2 + (a_1 g_{\sigma N}^2 \sigma^2 + b_1 g_{\omega N} \omega_\mu \omega^\mu) \vec{\rho}_\mu \cdot \vec{\rho}^\mu \quad (3)$$

In the above expressions, ψ_j describes baryon j , σ, σ^* are scalar-isoscalar meson fields, and $\omega^\mu, \phi^\mu, \vec{\rho}^\mu$ stand for the vector isoscalar and isovector fields, and $W_{\mu\nu}, P_{\mu\nu}, \vec{R}_{\mu\nu}$ are the vector meson field tensors $V_{\mu\nu} = \partial_\mu V_\nu - \partial_\nu V_\mu$.

The couplings $g_{\sigma N}, g_{\omega N}, g_{\rho N}$ in DD models are functions of the baryonic density fitted to nuclear matter properties, see [34, 35]. For NL models, the coupling constants $g_{\sigma N}, g_{\omega N}, g_{\rho N}, g_2, g_3, c_3, a_1, b_1$ and the σ, ω and ρ meson masses are fitted to experimental, theoretical and observational data.

Besides the RMF models described by the above Lagrangian density, we will also consider Skyrme forces in the next section, all predicting two solar mass stars. As a second constraint, we require that these models are still causal in the center of stars with a mass equal to $2M_\odot$. The values of the EoS parameters of these models at saturation density vary in a wide range of values and are given in [32, 4].

In the section on the hyperonic EoS, we will consider in the class of DD models the models DD2 [34] and DDME2 [35]. In the class of NL models we choose FSU2 [36], FSU2H and FSU2R [37, 38], NL3 [39], NL3 $\sigma\rho$ and NL3 $\omega\rho$ [40, 41], TM1 [42], TM1 $\omega\rho$ and TM1 $\sigma\rho$ [40, 43], TM1-2 and TM1-2 $\omega\rho$ [3]. Finally, in the last section, the models NL3 and NL3 $\omega\rho$ will be used.

Symmetry energy and neutron star radius and tidal deformability

In the present section we discuss the existing correlations between the neutron star radii, the tidal deformability, the Love number and several EoS parameters, or linear combinations of parameters, evaluated at saturation: the incompressibility K_0 , the skewness Q_0 , the slope of the incompressibility M_0 , the symmetry energy J_0 , its slope L_0 , and its

curvature $K_{\text{sym},0}$. In Ref. [32] it was shown that non-unified EoSs may introduce a large uncertainty on the determination of low-mass star radii, therefore, in the following we will consider full unified EoS for the Skyrme EoS and a unified inner crust-core EoS for the RMF models. For these models we have taken for the outer crust the EoS proposed in Ref. [44], and the EoS of the inner crust was calculated performing a Thomas Fermi calculation using the same model of the core EoS, see [45, 46]. For more details on this point please see Ref. [32, 47].

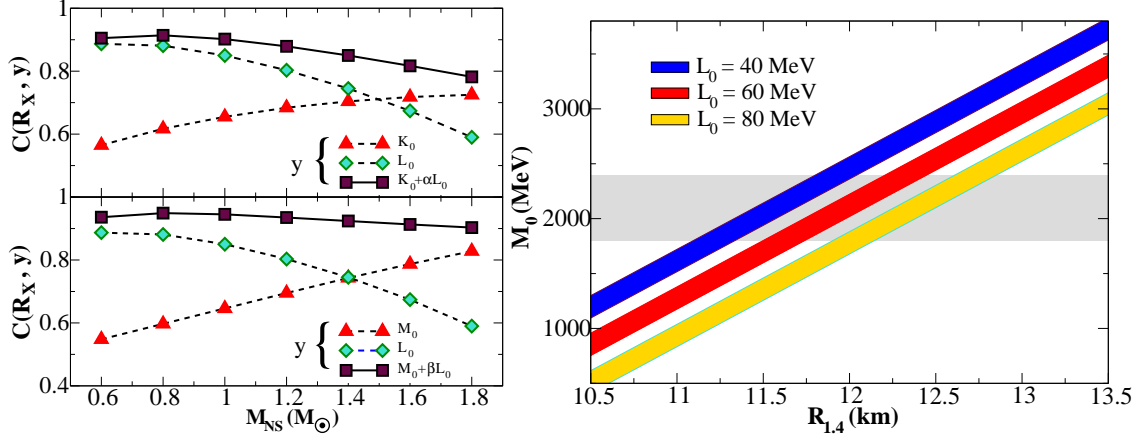


Figure 1. Left panel: The correlation coefficients between the neutron star radii and the ‘y’ EoS parameters as a function of the neutron star mass, where the ‘y’ parameters denote K_0 , L_0 , and $K_0 + \alpha L_0$ in the top panel, and M_0 , L_0 , and $M_0 + \beta L_0$ in the bottom panel. Right panel: M_0 as a function of $R_{1.4}$ for $L_0 = 40, 60$ and 80 MeV, as obtained from the multiple linear regression. The gray shaded region indicates the constraint on M_0 derived in Ref. [48]. Adapted from [47]

The linear correlation between any two quantities, a and b , will be calculated by the Pearson’s correlation coefficient, $C(a, b)$, given by

$$C(a, b) = \frac{\sigma_{ab}}{\sqrt{\sigma_{aa}\sigma_{bb}}}, \quad \text{with} \quad \sigma_{ab} = \frac{1}{N_m} \sum_i a_i b_i - \left(\frac{1}{N_m} \sum_i a_i \right) \left(\frac{1}{N_m} \sum_i b_i \right). \quad (4)$$

In this expression the index i runs over the N_m number of models [47, 17]. The quantities a_i and b_i correspond, respectively, to the neutron star radius for a fixed mass and an EoS parameter or a linear combination of two parameters.

In Fig. 1 we present, as a function of the star mass, results for the correlation between the radius and a) K_0 , L_0 and the linear combination $K_0 + \alpha L_0$, where α is chosen for each mass so as to give the largest correlation (top panel) and b) M_0 , L_0 and the linear combination $M_0 + \eta L_0$, where η and α are chosen in order to maximize the correlation. The correlation between L_0 and the radius is quite large only for low mass neutron stars. This same result was confirmed in [17]. For large masses a better correlation is obtained with the incompressibility K_0 at saturation or its slope M_0 . An improved correlation in the whole range of masses is obtained taking the combination $M_0 + \eta L_0$, or although not so strong, the combination $K_0 + \alpha L_0$. These results indicate that the knowledge of the EoS parameters, K_0 , M_0 and L_0 allows a good estimation of the star radius. In the right panel of Fig. 1, we demonstrate how we can obtain the star radius from L_0 and M_0 with the indication of uncertainties, taking $M_0 = 1800 - 2400$ [48] and L_0 within the range $40 < L_0 < 80$ MeV, as suggested by [7, 49] and [9]. In this figure, the incompressibility slope M_0 is plotted as a function of the $1.4M_\odot$ radius, $R_{1.4}$, for three values of the symmetry energy slope $L_0 = 40, 60$ and 80 MeV, and the gray shaded region denotes the constraint on M_0 determined in Ref. [48]. We have obtained $11.09 \lesssim R_{1.4} \lesssim 12.86$ consistent with others predictions as in Ref. [50, 51].

In [17] the Pearson correlations between the dimensionless tidal deformability $\Lambda = \frac{2}{3}k_2 \left(\frac{R}{M}\right)^5$ and Love number the k_2 [52] of stars with $1.2 \leq M \leq 1.6M_\odot$ have also been calculated for the same set of models. Only weak or moderate correlations have been obtained between Λ , k_2 and the EoS parameters. In Fig. 2, these correlations are shown for M_0 , L_0 and K_{sym} . However, similarly to the discussion above for the NS radius, also for the tidal deformability a strong correlation is determined with the linear combinations $M_0 + \beta L_0$ and $M_0 + \eta K_{\text{sym},0}$ over a wide range of NS masses. The parameters β and η are fixed so as to maximize the correlation and can be parametrized as $\beta = -1.90 + 265.02 \exp(-M/0.49)$ and $\eta = -1.4 + 29.81 \exp(-M/0.89)$, where M is the NS mass in units of solar

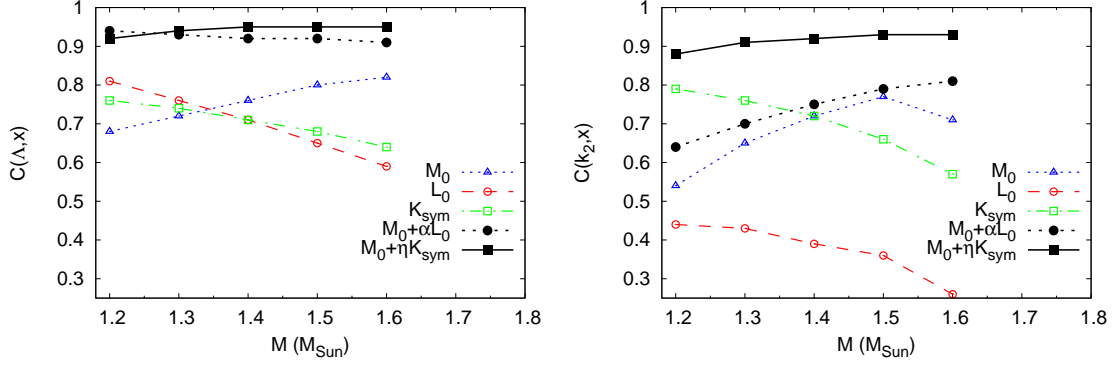


Figure 2. Pearson correlation coefficients for the correlations between the tidal deformability (left) and Love number k_2 (right), evaluated for NS with masses between 1.2 and 1.6 M_\odot , and the EoS properties: M_0 , L_0 and K_{sym} . Data from [17]

mass. Using the linear combination $M_0 + \eta K_{\text{sym},0}$ together with the upper and lower bounds on $\Lambda_{1.4}$ set, respectively, by the GW170817 detection [10, 13] and by the interpretation of its UV/optical/infrared counterpart, together with the empirical ranges of L_0 presented in Ref. [9], the values of M_0 and $K_{\text{sym},0}$ may be constrained to the intervals $1926 < M_0 < 3768$ MeV and $-140 < K_{\text{sym},0} < 16$ MeV [17]. .

Symmetry energy and hyperonic neutron stars

In the present section, we discuss the effect of the density dependence of the symmetry energy on the properties of hyperonic stars, in particular, on the direct Urca process (DU) both nucleonic and hyperonic, and on the onset of the different hyperonic species. The study will be undertaken applying the TM1 model [42] with an extra non-linear term that couples the ω and ρ -mesons allowing the change of the density dependence of the symmetry energy. We, therefore, generate a family of models with the same isoscalar properties but different isovector properties, e.g. the slope of the symmetry energy at saturation varies in the range $55 < L < 110$ MeV [43, 40].

The hyperon-meson couplings have been chosen so that: a) the coupling to the ρ -meson is defined by the isospin projection times nucleon- ρ -meson coupling; b) the couplings to the vector-mesons are fixed considering the SU(6) quark model prediction; c) the coupling Λ - σ -meson is fitted to hypernuclei data as in [33], for the Σ -meson we consider a set of the different couplings which we will discuss, and for the Ξ -meson we take the Ξ -potential in symmetric nuclear matter at saturation -18 MeV; d) we include the ϕ -meson but not the σ^* meson except for the Λ -hyperon.

We first discuss the nucleonic electron direct Urca (DU) process [53], the most efficient process when discussing the cooling on NS. In order to operate, both energy and linear momentum must be conserved. The second conservation law shifts the onset of this process to quite large densities due to the large neutron fraction together with a small proton fraction. In particular, the minimum proton fraction for the process to occur is $Y_p^{\text{min}} = \frac{1}{1+(1+x_e^{1/3})^3}$, with $x_e = n_e / (n_e + n_\mu)$, and n_e and n_μ the electron and muon densities. In the following, n_{DU} and mass M_{DU} designate, respectively, the baryonic density at which the DU process opens and the mass of the star with a central density equal to n_{DU} .

We perform the study within the RMF models presented in Section 1. These models fall in three different categories: a) models like TM1, NL3, FSU2, which have a large symmetry energy slope predict, the opening of the process at densities below the hyperon onset, corresponding to quite low mass stars; b) models like DD2 and DDME2 completely exclude this process inside the stars; c) models, like FSU2R, FSU2H, NL3 $\omega\rho$ or TM1 $\omega\rho$ with a symmetry energy slope below 75 MeV, predict the onset of the process above the onset of the hyperon onset.

In Fig. 3 we plot with open circles the onset density of the nucleonic electron DU as a function of the slope L for the family of TM1 $\omega\rho$ models. Since the proton fraction inside the star is defined by the density dependence of the symmetry energy, it results that there is a strong dependence of the DU onset on L , as previously discussed in [54, 2]. Models with a small L at saturation have smaller symmetry energies at supra-saturation densities, favor larger

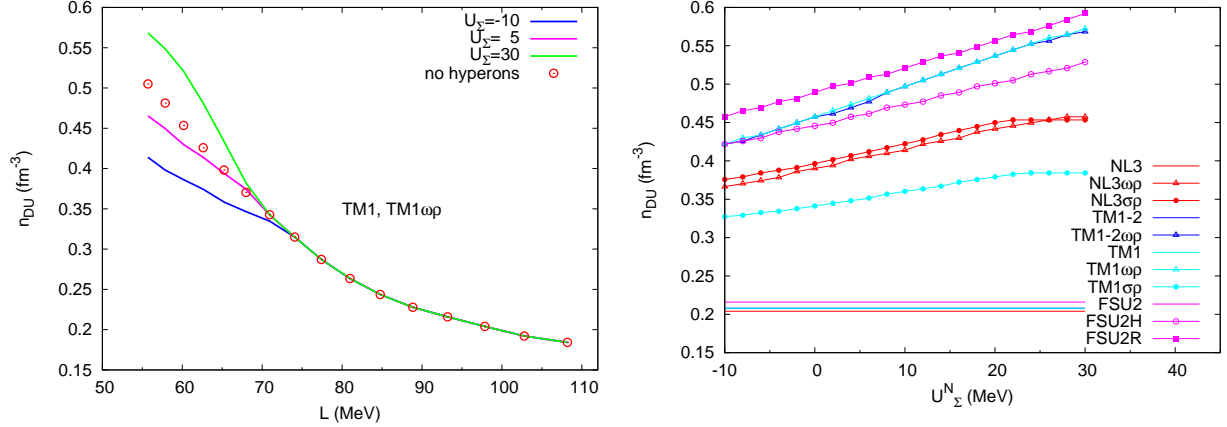


Figure 3. Direct Urca process onset density (left panel) as a function of the symmetry energy slope for the TM1 $\omega\rho$ models and several values of the Σ potential, U_Σ ; (middle panel) as a function of the U_Σ for several models that predict DUrca in the core of a NS; (right panel) the onset density of the different hyperonic species as a function of the symmetry energy for different values of U_Σ .

neutron-proton asymmetries and, as a consequence, disfavor the onset of DU at small densities.

In the presence of hyperons, channels for neutrino emission involving the hyperons are also possible [55]. Moreover, the hyperons will also affect the nucleonic electron DU process, because the fraction of electrons is strongly dependent on the presence of negatively charged hyperons. This is shown by the full lines in Fig. 3, which were calculated allowing for the appearance of hyperons, each one corresponding to a different Σ potential in symmetric nuclear matter. The effect is only present for $L \lesssim 75$ MeV: the more repulsive the Σ potential, the larger the onset density of the nucleonic DU. For an attractive or only slightly repulsive potential the onset of the DU process is smaller than the corresponding density for a pure nucleonic system. In fact, the Σ^- hyperon is the first to set in and, as a consequence, the proton fraction increases, the difference between the proton and neutron Fermi momenta decreases and the DU is favored [4]. For a more repulsive Σ potential, the Λ -hyperon sets in first. As soon as it appears neutrons, protons, electrons and muons all suffer a reduction, and the overall effect is to disfavor the DU process as compared to the pure nucleonic one.

The most efficient hyperonic DU processes are described by the equations:

$$\Sigma^- \rightarrow \Sigma^0 \ell^- \bar{\nu}_\ell, \quad R = 0.61 \quad (5)$$

$$\Xi^- \rightarrow \Xi^0 \ell^- \bar{\nu}_\ell, \quad R = 0.22 \quad (6)$$

$$\Sigma^- \rightarrow \Lambda \ell^- \bar{\nu}_\ell, \quad R = 0.21 \quad (7)$$

where the R factor indicates the efficiency of the process compared with the nucleonic DU process (see [55]). Two of the above processes, (5) and (7), involve a Σ hyperon, and, in particular, the first is three times more efficient than the other two. Determining if the Σ hyperon is present inside the NS and which is its abundances, is important to describe the cooling of a NS. Since this hyperon has isospin one, it is expectable that its presence is sensitive to the behavior of the symmetry energy.

In the right panel of Fig. 3 we plot the onset density of the nucleonic DU process as a function of the Σ potential for the set of models introduced in Section 1 (the DD models do not predict the nucleonic DU process). For models with a large L , as NL3, TM1 and FSU2, the onset density of DU, n_{DU} , does not depend on U_Σ because this density lies below the onset density of hyperons. For all the other models the more repulsive U_Σ the larger n_{DU} , and, as a consequence, the larger the mass of the NS where it becomes effective.

We finally comment on the effect of L on the hyperonic species inside the star, see Fig. 4. The Λ hyperon onset is practically not affected by the value of U_Σ , and, although its onset density increases slightly when L decreases, the mass of star at the Λ -onset is essentially independent of L and equal to $1.3M_\odot$. The effect of L on the hyperonic species inside the star can be summarized as follows: a) the onset of the Λ hyperon, which has zero isospin, is almost not affected by the density dependence of the symmetry energy; b) the contrary is true for the Σ^- and Ξ^- hyperons which have a non-zero isospin. For these hyperons their onset density decreases as L decreases. The Σ potential also

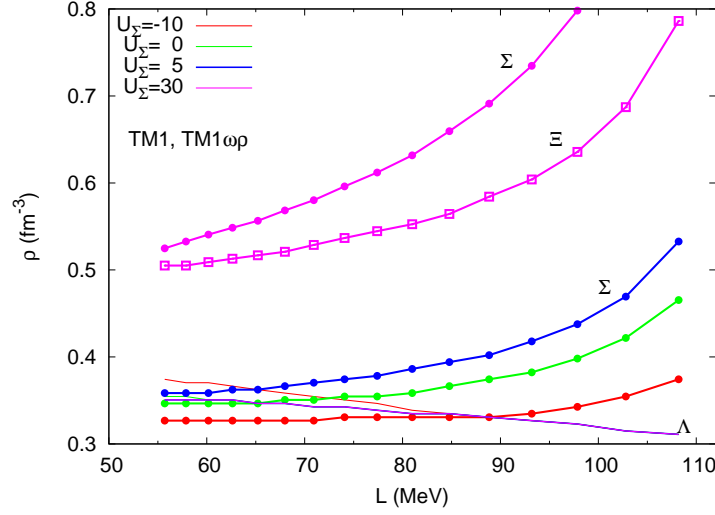


Figure 4. Onset density of the different hyperonic species, Σ (lines with dots), Ξ (lines with open squares), Λ (thin lines), as a function of the symmetry energy slope L for different values of the Σ potential U_Σ (given in MeV). The models TM1 and TM1 $\omega\rho$ have been used in the calculation.

influences the onset of the other species: the Ξ^- onset only occurs inside the NS if the Σ potential is very repulsive; the effect is larger for the smaller values of L when the onset density may be small enough to allow hyperons in stars with masses only slightly larger than $1M_\odot$.

As an application of the above results, in the following we discuss the effect of the U_Σ on the properties of NS described within the DDME2 model. In the left panels of Fig. 5 we plot in the bottom panel the onset densities of the Σ^- (yellow), Λ (pink) and Ξ^- (green), as well as the central baryonic density of the maximum mass star (black) and in the top panel the mass of the stars that have in the centre these same densities as a function of the Σ potential. As discussed before, the onset density for the Λ is insensitive to U_Σ . In this model the Σ^- sets in before the Λ for $U \lesssim +10$ MeV, and for $U \lesssim +30$, Ξ^- is the last hyperon to set in. In any case, the two solar mass constraint is satisfied and central densities are of the order of 1 fm^{-3} or just below. No nucleonic electron DU channel will open inside a NS, but the hyperonic DU process will be active as soon as the different species appear. In particular, the process described by Eq. (7) will be quite active above a density of the order of two times saturation density corresponding to a star with a mass $\sim 1.3M_\odot$.

In the right panel of Fig. 5, we show how the hyperon presence inside NS affects the cooling of the thermal state of NSs in Soft X-ray transients (SXT). In this panel we plot the luminosity in quiescence as a function of the accretion rate together with the observational data taken from [56], for purely nucleonic matter (black curves) and for different values of the Σ potential (dashed, dotted, and dot-dashed lines). We are interested in understanding the behavior of the SXT with the lowest-observed luminosity, SAX J1808.4-3658 [57, 58], indicated in red in the right panel. The upper black curve is obtained with the nucleonic EoS for the maximum mass star configuration. No DU process occurs and, therefore, it defines the lowest possible neutrino losses and the largest luminosity. The lower bounds were obtained with the hyperonic EoS, taking $U_\Sigma = -10, +10, +30$ MeV and considering the maximum mass configuration. These conditions define the largest neutrino emissions obtained through DU processes and, as a consequence, the lowest luminosity. Both results including a full accreted atmosphere or non-accreted one are shown. The low luminosity of the SAX J1808.4-3658 requires a very efficient neutrino emission processes operating in the core of the NS. A previous explanation for this low luminosity state required a quite hard EoS and a set of couplings of the hyperons to the mesons that favored the appearance of the complete baryonic octet in the NS core [59]. In contrast the present calculation explains the same state not requiring the nucleonic DU process, and not allowing for all the hyperon species, in particular, excluding the very efficient process described by Eq. (5), if no or only a small amount of accreted matter is in the envelope. Further investigation into this problem will be undertaken in the future.

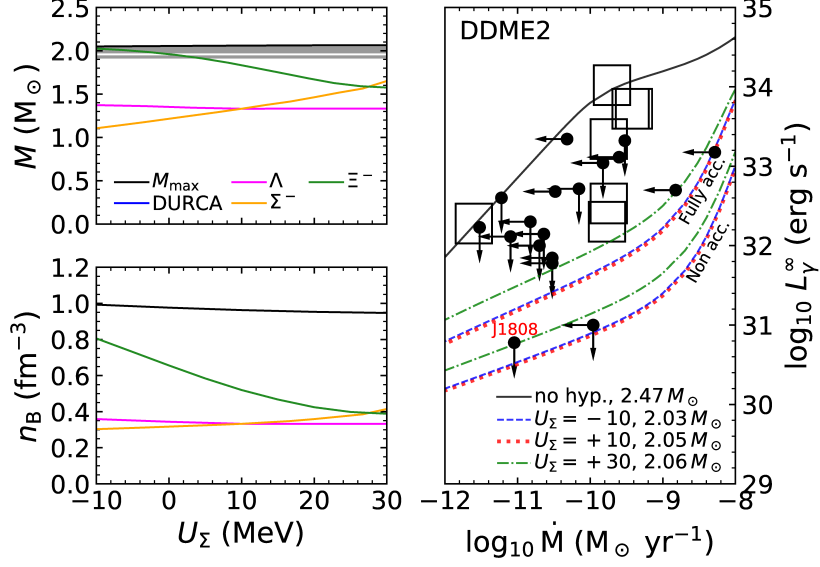


Figure 5. Left panels: onset densities of the different hyperons and NS central baryonic density of maximum mass star (bottom), mass of the NS with these densities at the center. Right panel: the luminosity of NSs in SXTs obtained for the maximum mass and with the nucleonic EoS (black curve) and several hyperonic EoS (colored lines) versus the observational data taken from [56]. The star indicated in red is the SAX J1808.4-3658 and has the lowest observed luminosity. Adapted from [4].

Symmetry energy and the crust-core transition of magnetized stars

In this section, we show how the crust-core transition in a NS is strongly affected by the magnetic field, and how the magnitude of this effect depends on the symmetry energy. For a zero magnetic field, it was shown that there is an anti-correlation between the transition density and the slope of the symmetry energy [60, 61, 62, 63, 64]. Since the magnetic field effects are sensitive to the amount of protons, we expect that the influence of the density dependence of the symmetry energy will reflect itself on the properties of the neutron star, specially in the range of small proton densities. Large proton densities require more intense magnetic fields to give rise to non-negligible effects. Inside a magnetar it is probable that the field intensity will be below 10^{18} G.

The crust-core transition is estimated from the calculation of the dynamical spinodal obtained within the relativistic Vlasov equation formalism applied to relativistic nuclear models [65]. It was shown that this method gives a good prediction of the crust core-transition in the absence of a magnetic field [66]. From the analysis of the dynamical spinodal, we conclude that the crust-core transition does not occur at a single density, but extends itself into a finite width range of densities [5]. Fig. 6 illustrates why this occurs. In this figure the dynamical spinodal section of nuclear matter at $B = 0$ (black curve) and for $B = 4.4 \times 10^{17}$ G (red curve) are shown in the $\rho_n - \rho_p$ plane. A complex structure of bands of unstable matter with large isospin asymmetry are present due to the filling of the Landau levels. In the same figure, we also plot the EoS of β -equilibrium stellar matter at zero temperature, and it is clearly seen that it crosses the spinodal section several times. If we associate the range of densities where these crossings occur to the transition region, we conclude that this region is formed by a series of alternating stable and unstable regions [5, 6].

In the right panel of Fig. 6, we plot the densities at the bottom and the top of the transition region (red lines in the top panel) and the radius of the corresponding neutron star layers as a function of the slope of the symmetry energy. We have considered a set of models based on the NL3 parametrization with an extra non-linear $\omega\rho$ term that introduces a density dependence on the symmetry energy [41]. The conversion of the density range into a neutron star layer was performed in an approximate way, by integrating the TOV equations for non-magnetized stars. In the future this approximation will be lifted. In the figures the solid black line corresponds to the results obtained taking $B = 0$. We conclude that the density and the radius of the bottom layer of the transition density is not much affected by the magnetic field, and the anti-correlation between the transition density and the symmetry energy slope is observed. The top layer of the transition density, only occurs for a non-zero magnetic field and its density and radius increases quite fast with the slope of the symmetry energy. For $L \sim 90$ MeV the transition region as a thickness of 0.06 fm^{-3} and

more than 1 km, reducing to 0.03 fm^{-3} and 400 m if $L = 60 \text{ MeV}$.

The increase of the crust thickness and of the complexity of the crust core transition region may have important consequences on the properties of neutrons stars, in particular, on the decay of the magnetic field, as discussed in [31] or on the glitch mechanism [29, 30].

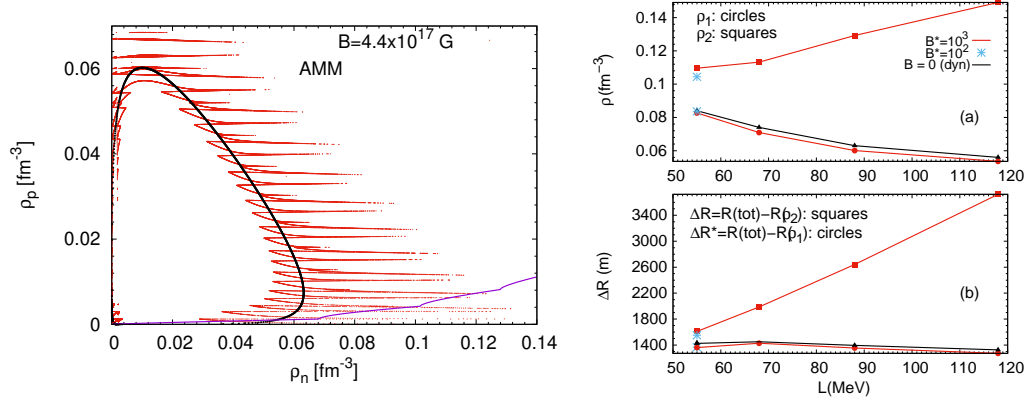


Figure 6. Left panel: the dynamical spinodal for nuclear matter obtained with $B = 0$ (black thick line) and $B = 4.4 \times 10^{17} \text{ G}$ (red curve). Also represented is the β -equilibrium EoS (purple line). Right panels: a) the transition densities, ρ_1 and ρ_2 and b) the crust thickness, ΔR , and $\Delta R^* = R(\text{tot}) - R(\rho_1)$ versus the symmetry energy slope L , obtained at $T = 0$ with $B^* = 10^3$ ($B = 4.4 \times 10^{16} \text{ G}$) (red) and $B = 0$ (black solid), within the dynamical spinodal formalism including the AMM. For $L = 55 \text{ MeV}$ also $B^* = 10^2$ ($B = 4.4 \times 10^{15} \text{ G}$) is shown (blue stars).

Conclusions

In the present review, we have shown how neutron star properties may set constraints on the EoS of asymmetric nuclear matter at both sub-saturation and high densities. We have analysed three different problems: the correlation between the NS properties, radius, tidal deformability and Love number, and several EoS parameters or linear combinations of parameters; the effect of the symmetry energy on the hyperonic content of neutron stars and on the DU process inside these stars; and the effect on the crust-core transition of magnetized neutron matter.

We could show that although the single parameters are generally, at most moderately correlated with those NS properties, some well chosen combinations of parameters are very well correlated. This linear combination together with other constraints either experimental or observational have allowed to set constraints on quantities as the slope of the incompressibility, M_0 and the curvature of the symmetry energy, K_{sym} [47, 17].

Concerning hyperonic stars, we have shown how the symmetry energy affects the nucleonic and the hyperonic direct Urca process. We have considered whenever possible constrained hyperon-meson couplings within a RMF framework [33]. Due to the lack of data on Σ -hypernuclei, we have also analysed how the hyperonic star properties depend on the Σ -potential. We have discussed the possibility of explaining the SXT with the lowest observed luminosity, SAX J1808, as an hyperonic star described by the DDME2 EoS [4], a RMF model with density dependent couplings 5.

A third problem addressed was the dependence of the crust-core transition in strongly magnetized matter on the density dependence of the symmetry energy [5, 6, 28]. The discussion was performed by applying the dynamic spinodal formalism. In the future, pasta calculations including the magnetic field effects need to be performed.

Acknowledgement

I would like to thank Morgane Fortin for preparing the Fig. 5. This work was supported by Fundação para a Ciência e Tecnologia, Portugal, under the projects UID/FIS/04564/2019 and POCI-01-0145-FEDER- 029912 with financial support from POCI, in its FEDER component, and by the FCT/MCTES budget through national funds (OE). Partial support comes also from the PHAROS COST Action CA16214.

Referências

- [1] B.-A. Li, A. Ramos, G. Verde, and I. Vidana, *Eur. Phys. J.*, A50, 9 (2014).
- [2] R. Cavagnoli, D. P. Menezes, and C. Providencia, *Phys. Rev.*, C84, 065810 (2011).
- [3] C. Providencia and A. Rabhi, *Phys. Rev.*, C87, 055801 (2013).
- [4] C. Providencia, M. Fortin, H. Pais, and A. Rabhi, *Frontiers in Astronomy and Space Sciences*, 6, 13 (2019).
- [5] J. Fang, S. Avancini, H. Pais, and C. Providencia, *Phys. Rev.*, C94, 062801 (2016).
- [6] J. Fang, H. Pais, S. Pratapsi, S. Avancini, J. Li, and C. Providencia, *Phys. Rev.*, C95, 045802 (2017).
- [7] M. B. Tsang *et al.*, *Phys. Rev.*, C86, 015803 (2012).
- [8] J. M. Lattimer and Y. Lim, *Astrophys. J.*, 771, 51 (2013).
- [9] M. Oertel, M. Hempel, T. Klöhn, and S. Typel, *Rev. Mod. Phys.*, 89, 015007 (2017).
- [10] B. P. Abbott *et al.*, *Phys. Rev. Lett.*, 119, 161101 (2017).
- [11] B. P. Abbott *et al.*, *Phys. Rev. Lett.*, 121, 161101 (2018).
- [12] D. Radice, A. Perego, F. Zappa, and S. Bernuzzi, *Astrophys. J.*, 852, L29 (2018).
- [13] S. De, D. Finstad, J. M. Lattimer, D. A. Brown, E. Berger, and C. M. Biwer, *Phys. Rev. Lett.*, 121, 091102 (2018). [Erratum: *Phys. Rev. Lett.* 121, 259902(2018)].
- [14] Z.-Y. Zhu, E.-P. Zhou, and A. Li, *Astrophys. J.*, 862, 98 (2018).
- [15] I. Tews, J. Margueron, and S. Reddy, *Phys. Rev.*, C98, 045804 (2018).
- [16] Y. Lim and J. W. Holt, *Phys. Rev. Lett.*, 121, 062701 (2018).
- [17] T. Malik, N. Alam, M. Fortin, C. Providencia, B. K. Agrawal, T. K. Jha, B. Kumar, and S. K. Patra, *Phys. Rev.*, C98, 035804 (2018).
- [18] F. J. Fattoyev, J. Piekarewicz, and C. J. Horowitz, *Phys. Rev. Lett.*, 120, 172702 (2018).
- [19] N.-B. Zhang and B.-A. Li, *Eur. Phys. J.*, A55, 39 (2019).
- [20] P. Demorest, T. Pennucci, S. Ransom, M. Roberts, and J. Hessels, *Nature*, 467, 1081 (2010).
- [21] Z. Arzoumanian *et al.*, *Astrophys. J. Suppl.*, 235, 37 (2018).
- [22] J. Antoniadis *et al.*, *Science*, 340, 6131 (2013).
- [23] I. Vidana, D. Logoteta, C. Providencia, A. Polls, and I. Bombaci, *EPL*, 94, 11002 (2011).
- [24] D. Chatterjee and I. Vidaa, *Eur. Phys. J.*, A52, 29 (2016).
- [25] I. Bednarek, Haensel, J. L. Zdunik, M. Bejger, and R. Manka, *Astron. Astrophys.*, 543, A157 (2012).
- [26] S. Weissenborn, D. Chatterjee, and J. Schaffner-Bielich, *Phys. Rev.*, C85, 065802 (2012); [Erratum: *Phys. Rev.* C90, 019904 (2014)].
- [27] S. Weissenborn, D. Chatterjee, and J. Schaffner-Bielich, *Nucl. Phys.*, A914, 421 (2013).
- [28] J. Fang, H. Pais, S. Pratapsi, and C. Providencia, *Phys. Rev.*, C95, 062801 (2017).
- [29] N. Andersson, K. Glampedakis, W. C. G. Ho, and C. M. Espinoza, *Phys. Rev. Lett.*, 109, 241103 (2012).
- [30] N. Chamel, *Phys. Rev. Lett.*, 110, 011101 (2013).
- [31] J. A. Pons, D. Viganò, and N. Rea, *Nature Phys.*, 9, 431 (2013).
- [32] M. Fortin, C. Providencia, A. R. Raduta, F. Gulminelli, J. L. Zdunik, Haensel, and M. Bejger, *Phys. Rev.*, C94, 035804 (2016).
- [33] M. Fortin, S. S. Avancini, C. Providencia, and I. Vidaa, *Phys. Rev. C*, 95, 065803 (2017).
- [34] S. Typel, G. Röpke, T. Klöhn, D. Blaschke, and H. Wolter, *Phys. Rev.*, C81, 015803 (2010).
- [35] G. A. Lalazissis, T. Niksić, D. Vretenar, and Ring, *Phys. Rev. C*, 71, 024312 (2005).
- [36] W.-C. Chen and J. Piekarewicz, *Phys. Rev.*, C90, 044305 (2014).
- [37] L. Tolos, M. Centelles, and A. Ramos, *Publ. Astron. Soc. Austral.*, 34, e065 (2017).
- [38] R. Negreiros, L. Tolos, M. Centelles, A. Ramos, and V. Dexheimer, *Astrophys. J.*, 863, 104 (2018).
- [39] G. A. Lalazissis, J. König, and Ring, *Phys. Rev.*, C55, 540 (1997).
- [40] H. Pais and C. Providencia, *Phys. Rev.*, C94, 015808 (2016).
- [41] C. J. Horowitz and J. Piekarewicz, *Phys. Rev. Lett.*, 86, 5647 (2001).
- [42] Y. Sugahara and H. Toki, *Nucl. Phys.*, A579, 557 (1994).
- [43] S. S. Bao and H. Shen, *Phys. Rev.*, C89, 045807 (2014).
- [44] S. B. Ruester, M. Hempel, and J. Schaffner-Bielich, *Phys. Rev.*, C73, 035804, (2006).
- [45] F. Grill, C. Providencia, and S. S. Avancini, *Phys. Rev.*, C85, 055808 (2012).
- [46] F. Grill, H. Pais, C. Providencia, I. Vidaa, and S. S. Avancini, *Phys. Rev.*, C90, 045803 (2014).
- [47] N. Alam, B. K. Agrawal, M. Fortin, H. Pais, C. Providencia, A. R. Raduta, and A. Sulaksono, *Phys. Rev.*, C94, 052801 (2016).
- [48] J. N. De, S. K. Samaddar, and B. K. Agrawal, *Phys. Rev.*, C92, 014304 (2015).

- [49] J. M. Lattimer and Y. Lim, *Astrophys. J.*, 771, 51 (2013).
- [50] B.-A. Li and A. W. Steiner, *Phys. Lett.*, B642, 436 (2006).
- [51] A. W. Steiner, J. M. Lattimer, and E. F. Brown, *Eur. Phys. J.*, A52, 18 (2016).
- [52] T. Hinderer, *The Astrophysical Journal*, 677,1216 (2008).
- [53] J. M. Lattimer, C. J. Pethick, M. Prakash, and Haensel, *Physical Review Letters*, 66, 2701 (1991).
- [54] C. J. Horowitz and J. Piekarewicz, *Phys. Rev. C*, 66, 055803 (2002).
- [55] M. Prakash, M. Prakash, J. M. Lattimer, and C. J. Pethick, *Astrophys. J.*, 390, L77 (1992).
- [56] M. V. Beznogov and D. G. Yakovlev, *Monthly Notices of the Royal Astronomical Society*, 447, 1598 (2015).
- [57] S. Campana, L. Stella, F. Gastaldello, S. Mereghetti, M. Colpi, G. L. Israel, L. Burderi, T. D. Salvo, and R. N. Robba, *The Astrophysical Journal Letters*, 575, L15 (2002).
- [58] C. O. Heinke, G. Jonker, R. Wijnands, C. J. Deloye, and R. E. Taam, *The Astrophysical Journal*, 691, 1035 (2009).
- [59] D. G. Yakovlev and C. J. Pethick, *Ann. Rev. Astron. Astrophys.*, 42, 169 (2004).
- [60] I. Vidana, C. Providencia, A. Polls, and A. Rios, *Phys. Rev.*, C80, 045806 (2009).
- [61] J. Xu, L.-W. Chen, B.-A. Li, and H.-R. Ma, *Astrophys. J.*, 697, 1549 (2009).
- [62] C. Ducoin, J. Margueron, and C. Providencia, *EPL*, 91, 32001 (2010).
- [63] C. Ducoin, J. Margueron, C. Providencia, and I. Vidana, *Phys. Rev.*, C83, 045810 (2011).
- [64] W. G. Newton, M. Gearheart, and B.-A. Li, *Astrophys. J. Suppl.*, 204, 9 (2013).
- [65] C. Providencia, L. Brito, S. S. Avancini, D. P. Menezes, and Chomaz, *Phys. Rev.*, C73, 025805 (2006).
- [66] S. S. Avancini, S. Chiacchiera, D. P. Menezes, and C. Providencia, *Phys. Rev.*, C82, 055807 (2010). [Erratum: *Phys. Rev.*C85,059904(2012)].